

Visual Statistics of the Total Geomagnetic Field Power



Sergey V. Starchenko and Svetlana V. Yakovleva

Abstract We carried out exploratory statistical and probabilistic analyzes of power $P = dE/dt$ of the observable potential geomagnetic field, where E is the total energy of the field. The field are taken from the geomagnetic model COV-OBS. $\times 1$ 1840–2020. The power is predominantly negative and takes values from -507 to $+117$ MW. Despite the extreme variability of the power P , its absolute value is three to four orders of magnitude smaller than the power required to maintain the geodynamo. The distribution function or, in other words, power spectrum is multimodal and its most significant almost flat part is in the range from -200 to -50 MW corresponding to the almost discrete spectrum of the energy. These main features and other statistical-probabilistic results are consistent with geomagnetic and geodynamo models, both in terms of the variability of the dipole field and of corresponding characteristic time scales, which are mostly of the order of a thousand years. We highlight a significant separate probabilistic mode with a power of about 500 MW, which may be associated with field variations with the duration of ~ 500 years.

Keywords Geomagnetic energy · Mathematical statistics · Distribution function · Geodynamo model

1 Introduction

Global variations of the observed geomagnetic field are most adequately described by variations of the integral energy of the observed potential part of the main geomagnetic field E .

The study of the energy of the potential part of the main geomagnetic field was initiated in [1]. Based on this work, Lowes [2] determined the normalized (by the area of the sphere and expressed in terms of T^2) contribution of the n -th harmonics

S. V. Starchenko (✉) · S. V. Yakovleva

Ionosphere and Radio Wave Propagation, Russian Academy of Sciences (IZMIRAN), Pushkov Institute of Terrestrial Magnetism, Kaluzhskoe Hwy. 4, Troitsk, Moscow 108840, Russia
e-mail: sstarchenko@mail.ru

responsible for multipoles in the radial energy density through the standard Gaussian coefficients (g_n^m, h_n^m), the radius of the Earth a and the spherical radius r .

$$R_n = (n + 1) \left(\frac{a}{r}\right)^{2n+4} \sum_m^n [(g_n^m)^2 + (h_n^m)^2]. \quad (1)$$

This expression was called by Lowes [2] the spatial power spectrum by analogy with a time varying ‘signal’, a plot of ‘power’ R , against ‘frequency’ n , whereas in reality it should be more correctly named the energy density spectrum and expressed in J/m. This density is variable of r , while the total energy is not. To obtain the total field energy, we first define correctly the non-normalized (in J/m) contribution of the n -th harmonics to the radial energy density of the potential field under consideration as.

$$\frac{4\pi r^2}{2\mu_0} R_n = 2\pi a^2 \frac{n+1}{\mu_0} \left(\frac{a}{r}\right)^{2(n+1)} \sum_{m=0}^n [(g_n^m)^2 + (h_n^m)^2]. \quad (2)$$

Finally, integrating (2) along the radius from the core-mantle boundary $r = c$ to infinity, in a physically obvious way, we get the contribution of the n -harmonics to the total energy (in J) together with the total energy as

$$\begin{aligned} E_n &= 2\pi a^{2n+4} \frac{n+1}{\mu_0} \sum_{m=0}^n [(g_n^m)^2 + (h_n^m)^2] \int_c^{+\infty} \frac{dr}{r^{2n+2}} \Rightarrow E_n \\ &= \frac{2\pi a^3}{\mu_0} \left(\frac{a}{c}\right)^{2n+1} \frac{n+1}{2n+1} \sum_{m=0}^n [(g_n^m)^2 + (h_n^m)^2], \quad E = \sum_{n=1}^N E_n. \end{aligned} \quad (3)$$

The resulting E_n is expressed in Joules and represents the total contribution of the harmonics of the degree n to the total energy of the potential field by integrating the radial energy density (known as the power spectra) along the radius from the core-mantle boundary ($r = c$) to infinity (see [3] for further details).

We tested this representation of E in detail [3, 4] on several global geomagnetic models [5–8]. The tests revealed that the energy variations are $\sim 10\%$, and are similar for all models except for the “splash” of the IGRF model in 1945–1950. We therefore excluded the IGRF model from further investigation due to its large five-year discreteness and imperfection of the determination of spectral harmonic (SH) coefficients of high degrees. The jumps in time variations in the period 1945–1955 are in particular need of explanation. Such unusual behavior was also noted in [9].

The *gufm1* historical model [6], which is still the most widely recognized, covers 400 years (from 1590 to 1990). This model is based on a large number of historical observations, i.e., of declination measurements and a small number of inclination measurements that were mainly made on ships for navigational purposes. The shortcoming of this model as well as other historical models is that, prior to 1840, they were based only on observations of magnetic field directions due to the absence of direct observations of the intensity before that time. The use of only observations of directions makes it possible to investigate the field morphology, but does not give

information of its absolute value which determines the energy. In the *gufm1* model, the axial dipole of the period from 1590 to 1840 is represented by a linear trend for 1840–1990. However, the secular variation has changed significantly since 1840, so there is no reason to assume that it was constant in earlier times.

In this study, we use COV-OBS. $\times 1$ (up to the highest degree $N = 14$, see the last equation in formula (3)) as one of the most successful global geomagnetic models [7, 8]. The model is based on a stochastic approach that integrates some preliminary information on the temporal evolution of the geomagnetic field through time covariance functions. The 1840–2020 model has a 6-month discreteness and is based on observatory and satellite data. The time series of SH coefficients are determined as realizations of a continuous and differentiable stochastic process. The model differs from regularized field models in that information contained in the observations is supplemented with stochastic, a priori information derived from the time spectra of geomagnetic series according to Gillet et al. [7].

The first three dipole coefficients, which are determined everywhere with a total error of less than 0.1%, make the main contribution to the energy E . The derivative (or P) is determined by the corresponding derivatives of the first 15 Gaussian coefficients (dipole, quadrupole, and octupole [3]) with an aggregate error of less than one percent of the root-mean-square (RMS) values.

The main goal of this study is the statistical-probabilistic analysis of the first time-derivative of the global energy E , hereafter referred to as power:

$$P \equiv \frac{dE}{dt}. \quad (4)$$

The statistical-probabilistic analysis of the power P is presented in Sect. 2. Statistical studies of P were carried out using experimental data analysis or ‘exploratory’ analysis techniques introduced by Tukey [10]. These methods are still very exotic for geophysics and possibly for a number of other natural sciences. Such procedures provide a visual overview of the nature of the data and, thus provide information about unusual distributions, and about appearance of extreme and even erroneous values in the dataset. The two most commonly used tools for such analysis are the “Stem and Leaf Plot” and the “Box Plot” [11].

The ratio of the introduced above discrete value of the energy E to the significant values of the powers P from (4) gives the characteristic times (or timescales), which are investigated and interpreted in Sect. 3 together with the summarized statistical-probabilistic results for P and E . Besides, in this section we compare our main statistical and probabilistic results with historical, paleomagnetic and geodynamo models, in terms of both the variability of the dipole field and the corresponding characteristic times. In accordance with this study and many others, the primary (more probable or those with the largest amplitude) timescales are of the order of a thousand years, while the secondary (less probable) ones are of the order of a hundred years.

Finally, Sect. 4 presents a brief discussion and summarizes the results of this study.

2 Evolution and Statistics of the Power P

We used 361 half-annual values of energy E obtained from the open source (<http://www.spacecenter.dk/files/magnetic-models/COV-OBSx1>) geomagnetic model COV-OBS. $\times 1$ [7, 8]. It spans 1840–2020 and is based on annual initial data. The authors of the model successfully extrapolated it down to the half-year resolution which is used here. In this work we calculate 180 annual P values from 361 half-annual E values presented in [3]. We used these E values to estimate the annual time-derivative $dE/dt = P$. It was calculated for each year as a ratio $[E(t - yr/2) - E(t + yr/2)]/yr$. Here t is the particular year and yr is 1 year. The values obtained for power P are then arranged in increasing order and thereafter referred as P_k , with k running from 1 to $K = 180$. The resulting cumulative distribution function of the sorted P_k values together with the initial evolution of the power $P(t)$ is shown in Fig. 1.

A stem-leaf diagram determined following the idea of the “Stem and Leaf Plot” [11] is presented in Table 1 for a detailed statistical-probabilistic analysis. The first one or two digits specify the class interval, called the “stem”, and the next digit (rounded if necessary) is used to construct increments of the bar which are called

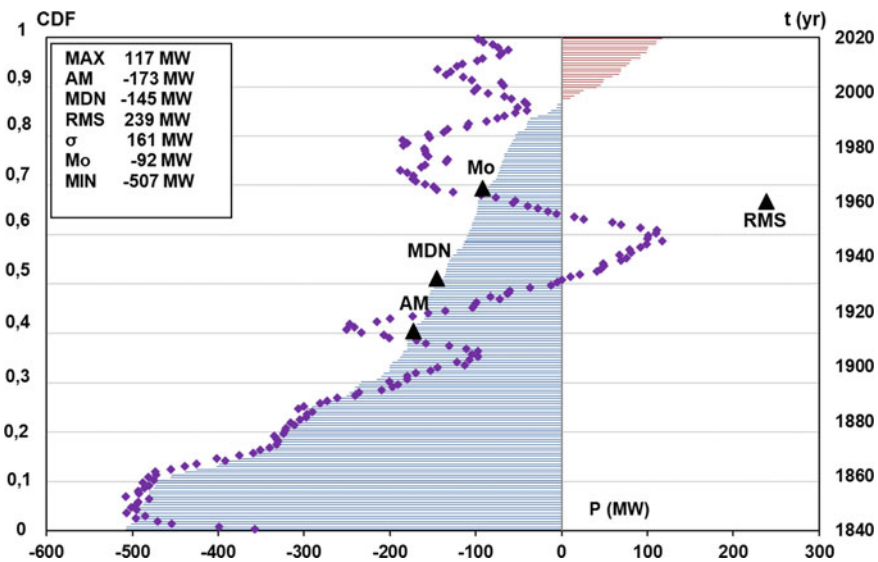


Fig. 1 Cumulative distribution function CDF and evolution of power P . CDF in the form of histogram and evolution of power (diamonds) are plotted along the horizontal axis in MW. The left vertical axis is dimensionless. It shows the probability that the value of the power P is equal or less than the value of the argument of the CDF. The right vertical axis t in years shows the evolution interval of $P(t)$. Main statistical parameters are shown as triangles and in the table in the upper left corner: MAX—maximum value, AM—arithmetic mean, MDN—median, RMS—root-mean-square, σ —standard deviation, Mo—mode or most probable value, MIN—minimum value

the “leaves”. As the “stem” (the leftmost column), we use the power values with increments of 50 MW for each row or “branch”. Within each such line, five ($D = 0, 1, 2, 3, 4$ or $5, 6, 7, 8, 9$) different implementations or “leaves” are possible. They are represented by the multiples of 10 MW, which are respectively added or subtracted from the “stem” value. The largest number of realizations (31) falls on the “branch” with 9 values close to -90 MW. The last value encountered most frequently corresponds to the most probable value $M_o = -92$ MW, which is naturally defined as the average of all realizations corresponding to the “leaves” indicated by the number 9 in the “branch” with 31 realizations.

Demonstration of individual data points is the major advantage of this representation. Besides, we see individual distributions of those data in each diagram “branch” that is not seen in histogram (e.g., in Fig. 2 below). We believe that our conclusions will be not affected by a minor change of the temporal resolution, which is one year for the model considered in this study, though a more detailed analysis of this issue would require additional research. We see some advantages of the stem-and-leaf diagram over histograms (compare Table 1 with Fig. 2) when the amount of data is relatively small, and one could distinguish individual points, as in this study.

We now proceed to mostly qualitative but nevertheless very clear graphical analyzes which are based on Table 1 and are presented in Fig. 2 as a histogram and a box-plot. Hereinafter, a histogram means a step function St of the probability distribution. The height of each column of the histogram (or, equivalently, the value

Table 1 Stem-leaf diagram for power P (in MW)

Stem S	“Branches” (rows) with “leaves” (digits $D \mid P = S \pm 10D$)	i	AM
100+	0 1 1 1	4	110
0+	5 6 6 6 7 7 8 9 9 9 9	11	80.4
0+	0 1 1 2 2 4 4 4 4	9	28.5
0–	0 0 1 1 2 3 3 4 4 4	10	-26.5
0–	5 5 5 5 5 6 6 6 6 6 6 6 6 7 7 7 7 7 8 8 8 8 8 9 9 9 9 9 9 9 9	31	-76.5
-100–	0 0 0 0 0 0 1 1 1 1 1 2 2 2 2 3 3 3 3 3 3 4 4 4 4	27	-123
-100–	5 5 5 5 5 5 5 5 5 6 6 6 7 7 7 7 7 7 7 8 8 8 8 8 9 9 9	28	-171
-200–	0 0 0 0 1 3 3 4 4 4	10	-223
-200–	5 6 7 8 9 9 9	7	-279
-300–	0 0 0 1 1 2 2 2 3 3 3 3 4	13	-321
-300–	5 5 5 7 9 9	6	-372
-400–	0 2 4	3	-422
-400–	7 7 7 7 8 8 8 8 8 8 9 9 9 9 9 9 9	18	-482
-500–	0 1 1	3	-505
	All	180	

Note i is the number of “leaves” in each “branch”, AM is the arithmetic mean (in MW). A fixed increment or the width of a column of the histogram is 50 MW. The exact value of an individual data point can be obtained from the expression at the top of column 2

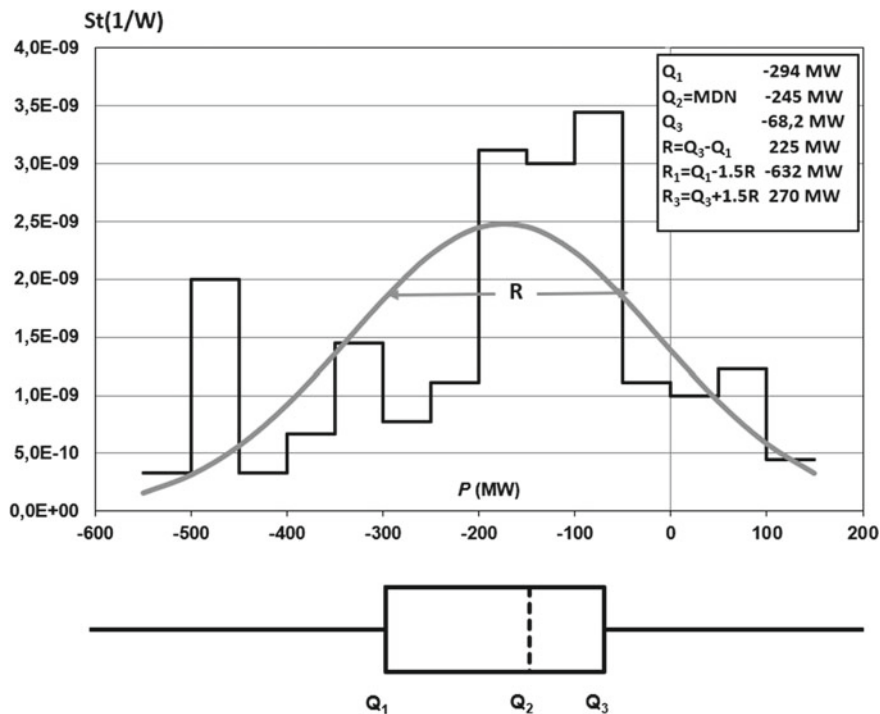


Fig. 2 Step function (St) of the probability distribution of P . The dimension along the vertical axis is $1/W$. The normal distribution function (solid curve) with the same mean and standard deviation is shown. The box plot is presented below. The main statistical parameters are shown in the upper right corner. Q_1, Q_2, Q_3 are the endpoints corresponding to the first, second, and third quartiles, $R = Q_3 - Q_1$ is the range between the first and third quartiles. The dashed vertical line inside the box at Q_2 indicates the median. Horizontal lines that radiate from the box represent the range of observed values inside the “inner fences”, which are located at 1.5 times the value of the interquartile range ($1.5R$) beyond Q_1 to the left and Q_3 on the right. The numerical values of these quantities are given in the upper right corner of the figure

of each step of the distribution function) is obtained from the corresponding row (“branch”) in Table 1 by dividing the number of realizations or “leaves” i inside the “branch” by the total number (180) of realizations and by a fixed (50 MW) increment, the width of a column of the histogram. The step function is then written as $St(b) = i(b)/(180 \cdot 50MW)$, where b is the number of a branch counted from the bottom to the top in Table 1. At the same time, the normalization condition is obviously fulfilled: the integral of the histogram (precisely the sum of all $St(b)$ values multiplied by 50 MW) over the energy range from -600 to 200 MW is equal to 1, because the sum of all i indices is equal to 180, i.e., to the area under the distribution function. The normal distribution function (solid curve) with the same mean (AM) and standard deviation (σ) is shown in Fig. 2 for comparison.

For a visual interpretation of our statistical results, we present a box diagram (original name “Box Plot” [11]). It is shown at the bottom of Fig. 2. Following [11], the quartiles Q_1 and Q_3 are found by counting ($K/4$) leaf values from the top and bottom, respectively. These values also provide the interquartile range: $R = Q_3 - Q_1$ which is approximately equal to two standard deviations (2σ). The first quartile value Q_1 specifies the “left side of the box” limiting the first 25% of realizations, the second quartile value Q_2 corresponds to 50% of realizations and is equal to the median value MDN, and the third quartile value Q_3 specifies the “right side of the box” limiting the last 25% (see also Table 1). So, the “box” represents the interquartile range R and the endpoints Q_1 and Q_3 . To analyze the distribution outside the “box” we calculate endpoints R_2 and R_3 which are located at 1.5 times the value of the interquartile range ($1.5R$) beyond Q_1 to the left and Q_3 on the right. They form so called “inner fences”. Another two endpoints, R_1 and R_4 , are located at 3 times the value of the interquartile range ($3R$) beyond Q_1 to the left and Q_3 on the right and form so called “outer fences”.

In our case, all values of the series lying outside the “box” including the minimum and maximum values, turn out to be both inside the outer borders $R_1 = Q_1 - 3R$ and $R_4 = Q_3 + 3R$ as well as inside the inner borders $R_2 = Q_1 - 1.5R$ and $R_3 = Q_3 + 1.5R$, so these borders are not displayed. Straight lines indicate the so called “whiskers”, i.e., a set of values of the series that lie outside the box, but do not extend beyond the inner border.

As follows from Fig. 2, the mean, median and most probable value (mode) are concentrated in the range from -200 to -50 MW and form an almost flat part of the step function. The RMS value is equal to 239 MW and lies beyond the upper limit (naturally, we compare the absolute values) of this range, which indicates the probability of formation of “heavy” tails. Formally, the power P does not deviate significantly from the normal distribution; however, four local modes are clearly distinguished in Fig. 2 showing that the actual distribution is multimodal with a number of modes depending on the bin size.

3 Statistics and Characteristic Timescales

The major statistical parameters of power P are summarized in the Table 2. For comparison we added the statistical parameters of energy E . All the parameters were calculated from their standard definitions. Additionally, negative and positive powers P are considered separately in two bottom rows of the table. About 86% of P values are negative and indicate the dominant decreasing trend in the energy E . The remaining 14% indicate rather short-term energy increases.

The main statistical feature of the energy E , as seen from the Table 2, is its extremely high ($SD/RMS < 0.04$) concentration near the practically coinciding values of Mo and MDN. Therefore, it seems acceptable to assume that the energy value tends to stabilization near a certain selected level. On the contrary, the relative deviation of the total power is very large ($SD/RMS = 0.67$, row $P(W)$ in Table 2). This fact

Table 2 Statistical parameters of the energy E and power P

Range	Total number(J for E , K for P)	Minimum (MIN), median (MDN), maximum (MAX)			Arithmetic mean (AM), Root mean square (RMS), Standard deviation (SD), Mode (Mo)			
		MIN	MDN	MAX	AM	RMS	SD	Mo
$E(J)$	361	$6.64 \cdot 10^{18}$	$6.85 \cdot 10^{18}$ $= F$	$7.62 \cdot 10^{18}$	$6.94 \cdot 10^{18}$	$6.94 \cdot 10^{18}$	$2.46 \cdot 10^{17}$	$6.85 \cdot 10^{18}$ $= F$
$P(W)$	180	$-5.07 \cdot 10^8$	$-1.45 \cdot 10^8$	$1.17 \cdot 10^8$	$-1.73 \cdot 10^8$	$2.39 \cdot 10^8$	$1.61 \cdot 10^8$	$-9.22 \cdot 10^7$
$P > 0$	25	$3.65 \cdot 10^5$	$6.93 \cdot 10^7$	$1.17 \cdot 10^8$	$6.58 \cdot 10^7$	$7.24 \cdot 10^7$	$3.30 \cdot 10^7$	$6.96 \cdot 10^7$
$P < 0$	155	$-5.07 \cdot 10^8$	$-1.59 \cdot 10^8$	$-4.93 \cdot 10^6$	$-2.10 \cdot 10^8$	$2.56 \cdot 10^8$	$1.45 \cdot 10^8$	$-9.22 \cdot 10^7$

indicates an extremely high variability of power values. Such statistical feature of power is a consequence of the concentration of energy at some selected value, as power is the derivative of energy with respect to time. Despite the extreme variability of the power P , its absolute value is three to four orders of magnitude smaller than the power required to maintain the geodynamo estimated to be about 0.1–1 TW [12–16]. Thus, as already known, the internal (locked below the core-mantle boundary, and principally unobservable) field normally strongly dominates over the directly observable magnetic field studied in this paper.

At the same time, our $\text{RMS}(P) = 239$ MW is more than an order of magnitude higher than the power provided by the dissipation of currents responsible for generating a geomagnetic dipole. The dipole's power, for example, was estimated at about 15 MW by Starchenko and Smirnov [17]. Therefore, based on the assumption that the dipole component makes a significant contribution to the variations in our power P (see [3] for details), we can argue that the characteristic times obtained from the above energy and power statistics predominantly reflect the behavior of the geodynamo directly related to the conductive fluid flows, and not with less significant ohmic dissipation.

Next, we estimate the characteristic times (timescales) in terms of the ratio of energy E to power P . Those characteristic timescales are obtained from the simplest estimations that deal with the ratio of a value to its time derivative. Obviously, with such a 'quick-and-dirty' approach one could obtain timescales with durations far exceeding the initial length of the time series. The essence is that in this case we study a monotonic process, while timescales usually refer to a periodic or harmonic process. Such 'monotonic' timescales yield snapshots for a given epoch which might be extended to other epochs based on the ergodicity argument.

Let us start with the ratio $\text{RMS}(E)/\text{RMS}(P) = 925$ years. Based on the above argument about the almost permanent energy value over a sufficiently extended time interval, we divide this fixed value $F = 6.85$ EJ by various power values. This value of F , with an accuracy of 3 digits, gives the same MDN and Mo in the line starting with $E(\text{J})$ in Table 2.

We obtain the timescale of about 4 thousand years by dividing F by 50 MW. We use 50 MW because it corresponds to the right edge of the highest column of the probability distribution function in Fig. 2. Dividing F by 100, 150 and 200 MW, we obtain an almost flat or continuous main temporal spectrum for the interval from about thousand to four thousand years. Characteristic timescales of 10^3 – 10^4 years are obtained for the main geodynamo processes from observational, archaeo- and paleomagnetic evidence, and various geodynamo models [18–27].

Many authors [12–15, 18–24] assume the centennial characteristic timescales to be the next in importance or in "spectral weight". The same result occurs when dividing the F value by the power absolute value $|P|$, shown in Fig. 2 in the area where the power P is less than -200 MW. However, the column with the edges of -500 and -450 MW stands out as a significant separate probabilistic mode, corresponding to a timescale of ~ 500 years. However, the peak around -450 MW in Fig. 2 is entirely due to the first ~ 25 years of the record, as seen in Fig. 1. The limited length of the record might impact the results significantly. Starchenko and Yakovleva [4] recently

highlighted a similar feature, but in an even more striking form, within the framework of a different, exclusively temporal, statistical approach. Now, we obtain additional confirmation from the standpoint of energy and power statistics.

4 Discussion and Conclusion

The statistical study of the power $P = dE/dt$ carried out in this work is almost entirely exploratory, since it is primarily aimed at determining hypothetical regularities for predominantly nonrandom geodynamo processes. At the same time, we realize that we cannot claim a sufficiently high accuracy of the proposed hypotheses, since the studied 180-year series is too short in comparison with the most characteristic timescales of the geodynamo which are of the order of thousands of years. On the other hand, this time series is distinguished by incomparably more accurate dating and reliability of the direct instrumental determination of the values of E and P in comparison with rather long-term archeomagnetic and paleomagnetic models of the ancient field, reconstructed only hypothetically. Therefore, an exploratory research based on a short but sufficiently accurate series seems a reasonable approach to verify relatively long but rough archaeo- and/or paleomagnetic series and geodynamo models. In this way, we are able to obtain confirmation of our hypotheses, which are based on the natural assumption about the ergodicity of the processes under consideration.

Our study is in correlation with the work of Bouligand et al. [24], who investigated the statistical properties of the Gaussian coefficients on the basis of an even shorter but extremely accurate series of satellite observations, additionally using appropriately normalized long-term numerical geodynamo models. Bouligand et al. showed that all these coefficients, with the exception of the axial dipole, can be modeled by a stationary and differentiable stochastic process characterized by a single time scale. A similar statement about the nonrandom behavior of the axial dipole in historical models was justified by Hulot and Le Mouél [28].

In conclusion, we agree that the accuracy of our study is low, but it is based on direct instrumental measurements of the geomagnetic field. Therefore, this accuracy is not worse, but likely even better than the accuracy of intrinsically hypothetical reconstructions, which are the only alternative models of the past geomagnetic field and geodynamo at the timescales exceeding several hundred years. Verification and even estimation of this accuracy would certainly require extensive additional studies.

In the following, we formulate the main results of the presented study.

1. The main statistical feature of the total power is a significant SD/RMS relative deviation of 67% indicating an extremely high variability of the power values. Such statistical feature of power is a result of the concentration of energy at a certain constant value. Despite the extreme variability of the power P , its absolute value is three to four orders of magnitude less than the power (~ 0.1 – 1 TW) required to maintain the geodynamo.

2. The statistical properties of the power P primarily result from the almost flat part of its multimodal spectrum in the range from -200 to -50 MW, where the average, median and most probable values are concentrated. The RMS value is equal to 239 MW that is well above the absolute value of these quantities indicating the probability of formation of “heavy” tails in the power P distribution.
3. The ratio of the main discrete value F (as defined in Table 2) to the most significant derivatives or powers P yields characteristic times which are investigated and interpreted together with the summary statistical-probabilistic results for P and E . These statistical-probabilistic results agree with historical, paleomagnetic and geodynamo models in terms of both the variability of the dipole field and the corresponding characteristic times which are mostly of the order of a thousand years.
4. We highlight a significant separate probabilistic mode with a power of about $S = 0.5$ GW (seen in the left part of Fig. 2), which translates into a timescale of ~ 500 years according to the relation F/S . A similar feature, but in an even more striking form, was recently singled out by Starchenko and Yakovleva [4] within the framework of a different, exclusively temporal, statistical approach.

Acknowledgements The authors are grateful to IZMIRAN for financial assistance in the preparation of the article, and to three anonymous referees who helped us to improve this work significantly.

References

1. Mauersberger, P.: Das Mittel der Energiedichte des geomagnetischen Hauptfeldes an der Erdoberfläche und seine sakulare Änderung. *Gerlands Beitr. Geophys.* 65, 207–215 (1956).
2. Lowes, F.J.: Spatial power spectrum of the main geomagnetic field, and extrapolation to the core. *Geophys. J. R. Astr. Soc.* 36, 717–730 (1974).
3. Starchenko, S.V., Yakovleva, S.V.: Energy and power spectra of the potential geomagnetic field since 1840. *Geomagn. Aeron.* 59(2), 242–248 (2019).
4. Starchenko, S.V., Yakovleva S.V.: Two century evolution and statistics of times of variations in the energy of the potential geomagnetic field. *Geomagn. Aeron.* 61(5), 661–671 (2021).
5. Thébault, E., Finlay C.C., Beggan C.D. et al.: International Geomagnetic Reference Field: the 12th generation. *Earth, Planets and Space* 67, 79–98 (2015).
6. Jackson, A., Jonkers A.R.T., Walker M.R.: Four centuries of geomagnetic secular variation from historical records. *Phil. Trans. R. Soc. Lond.* A358, 957–990 (2000).
7. Gillet, N., Jault, D., Finlay, C.C., Olsen, N.: Stochastic modeling of the Earth’s magnetic field: inversion for covariances over the observatory era. *Geochem. Geophys. Geosyst.* 14(4), 766–786 (2013).
8. Gillet, N., Barrois, O., Finlay, C.C.: Stochastic forecasting of the geomagnetic field from the COV-OBS.x1 geomagnetic field model, and candidate models for IGRF-12. *Earth, Planet and Space* 67, 71 (2015).
9. Wen-yao, Xu.: Unusual behavior of the IGRF during the 1945–1955 period. *Earth Planets Space.* V. 52. P. 1227–1233 (2000).

10. Tukey, J.W.: *Exploratory Data Analysis*. Addison-Wesley Pub. Co., Reading, Massachusetts, USA (1977).
11. Freund, R.J., Mohr D.L., Wilson W.J.: *Statistical Methods*. 3d ed. Academic press, Salt Lake City, USA (2010).
12. Parkinson, W.D.: *Introduction to Geomagnetism*. Scottish Acad. Press, Edinburgh (1983).
13. Braginsky, S.I., Roberts P.H.: Equations governing convection in the Earth's core and the geodynamo, *Geophys. Astrophys. Fluid Dynamics* 79, 1–97 (1995).
14. Starchenko, S.V., Jones V.: Typical velocity and magnetic field strengths in planetary interiors. *Icarus* 157, 426–435 (2002).
15. Starchenko, S.V.: Analytic base of geodynamo-like scaling laws in the planets, geomagnetic periodicities and inversions. *Geomagn. Aeron.* 54(6), 694–701 (2014).
16. Starchenko, S.V.: Analytic scaling laws in planetary dynamo models. *Geophysical and Astrophysical Fluid Dynamics* 113(1–2), 71–79 (2019).
17. Starchenko, S.V., Smirnov A.Y.: Volume Currents of Present-Day Magnetic Dipole in the Earth's Core. *Izv., Phys. Solid Earth* 57, 474–478 (2021).
18. Braginsky, S.I.: Analytical description of the geomagnetic field of past epochs and determination of the spectrum of magnetic waves in the earth's core. *Geomagn. Aeron.* 14(3), 522–529 (1974).
19. Burakov, K.S., Galyagin D.K., Nachasova I.E., Reshetnyak M.Yu., Sokolov D.D., Frick P.G.: Wavelet analysis of geomagnetic field intensity for the past 4000 years. *Izvestiya, Physics of the Solid Earth* 34(9), 773–778 (1998).
20. Nachasova, I.E., Pilipenko O.V.: Archaeomagnetic studies at Schmidt institute of physics of the earth, russian academy of sciences: history and main results. *Izvestiya, Physics of the Solid Earth* 55(2), 298–310 (2019).
21. Starchenko S.V.: Harmonic sources of the main geomagnetic field in the earth's core. *Geomagn. Aeron.* 51(3), 409–414 (2011).
22. Starchenko, S.V., Yakovleva S.V.: Determination of specific time variations in the energy of the earth's magnetic potential field from the IGRF model. *Geomagn. Aeron.* 59(5), 606–611 (2019b).
23. Starchenko, S.V., Pushkarev Y.D.: Magnetohydrodynamic scaling of geodynamo and a planetary protocoore concept. *Magnetohydrodynamics* 49(1-2), 35–42 (2013).
24. Bouligand, C., Gillet N., Jault D., Schaeffer N., Fournier A., Aubert J.: Frequency spectrum of the geomagnetic field harmonic coefficients from dynamo simulations. *Geophysical Journal International* 207(2), 1142–1157 (2016).
25. Morzfeld, M., Buffett B.A.: A comprehensive model for the kyr and Myr timescales of Earth's axial magnetic dipole field. *Nonlinear Processes in Geophysics* 26(3), 123–142 (2019).
26. Panovska, S., Finlay C.C., Hirt A.M.: Observed periodicities and the spectrum of field variations in Holocene magnetic records. *Earth and Planetary Science Letters* 379, 88–94 (2013).
27. Panovska, S., Constable C.G., Korte M.: Extending global continuous geomagnetic field reconstructions on timescales beyond human civilization. *Geochemistry, Geophysics, Geosystems* 19(12), 4757–4772 (2018).
28. Hulot, G., Le Mouél J.L.: A statistical approach to the Earth's main magnetic field. *Physics of the Earth and Planetary Interiors* 82(3-4), 167–183 (1984).